

http://pubs.acs.org/journal/aesccq Article

Sensitivity Analysis and Uncertainty Quantification of PFAS Fate and Transport in Heterogeneous Riparian Sediments

Pei Li,* Jeffery T. McGarr, Farzad Moeini, Zhenxue Dai, and Mohamad Reza Soltanian*



Cite This: ACS Earth Space Chem. 2024, 8, 1560–1573



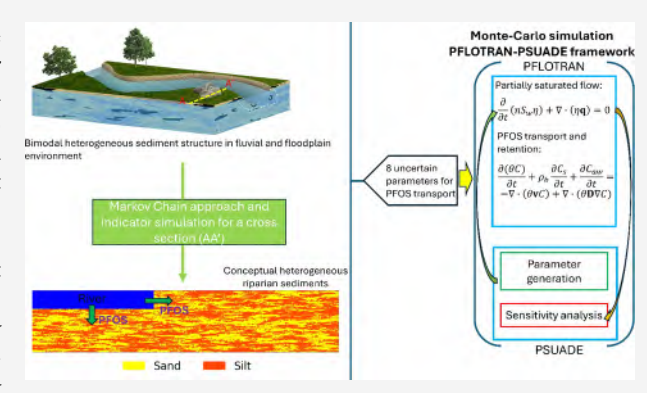
ACCESS I

III Metrics & More

Article Recommendations

Supporting Information

ABSTRACT: Per- and polyfluoroalkyl substances (PFAS) are surface-active contaminants, which are detected in groundwater globally, presenting serious health concerns. The vadose zone and surface water are recognized as primary sources of PFAS contamination. Previous studies have explored PFAS transport and retention mechanisms in the vadose zone, revealing that adsorption at interfaces and soil/sediment heterogeneity significantly influences PFAS retention. However, our understanding of how surface water—groundwater interactions along river corridors impact PFAS transport remains limited. To analyze PFAS transport during surface water—groundwater interactions, we performed saturated—unsaturated flow and reactive transport simulations in heterogeneous riparian sediments. Incorporating uncertainty quantification and sensitivity



analysis, we identified key physical and geochemical sediment properties influencing PFAS transport. Our models considered aqueous-phase transport and adsorption both at the air—water interface (AWI) and the solid-phase surface. We tested different cases of heterogeneous sediments with varying volume proportions of higher permeability sediments, conducting 2000 simulations for each case, followed by global sensitivity and response surface analyses. Results indicate that sediment porosities, which are correlated to permeabilities, are crucial for PFAS transport in riparian sediments during river stage fluctuations. High-permeable sediment (e.g., sandy gravel, sand) is the preferential path for the PFAS transport, and low-permeable sediment (e.g., silt, clay) is where PFAS is retained. Additionally, the results show that adsorption at interfaces (AWI and solid phase) has a small impact on PFAS retention in riparian environments. This study offers insights into factors influencing PFAS transport in riparian sediments, potentially aiding the development of strategies to reduce the risk of PFAS contamination in groundwater from surface water.

KEYWORDS: PFAS, PFOS, surface water—groundwater interactions, heterogeneity, riparian sediments, Monte Carlo simulation, sensitivity analysis, uncertainty analysis

INTRODUCTION

Per- and polyfluoroalkyl substances (PFAS) have been widely used in many industrial and consumer products globally due to their unique physical and chemical properties, with over 9000 PFAS compounds introduced to the market since their invention in the 1940s. 1-7 After being manufactured and used for more than 80 years, they are now ubiquitous in the environment (e.g., groundwater, soil, surface water) from sources such as landfills, wastewater treatment plants, industrial emissions, and agricultural lands.⁸⁻¹⁰ Due to their extremely strong carbon-fluorine bonds in the molecular structure, they are generally persistent in the environment, and their estimated half-life times are from decades to thousands of years. 9,11,12 It has been found that PFAS can increase the risk of cancers (e.g., prostate, kidney, and testicular cancers) and obesity, interfere with the body's natural hormones, and damage the body's immune system and reproductive function. 11-13 Therefore, they have become an emerging contaminant of concern in our drinking water resources. Based on the regional and global

sampling work, PFAS is frequently detected in groundwater, which is usually the local drinking water source. ^{1,9,14,15} As a result, it is important to understand PFAS fate and transport in a natural setting and its distribution among different phases (e.g., aqueous-phase and solid-phase surface).

A number of recent studies have demonstrated that the vadose zone is a source zone of PFAS. 16-18 Its complexity is the coexistence of fluid-fluid and fluid-solid interfaces. The primary interfaces in the vadose zone include air—water interfaces (AWI) within partially saturated conditions and the soil—water interface. PFAS can be adsorbed on both of them. 4,19,20 In the vadose zone, a multiphase and multi-

Received: February 21, 2024
Revised: July 22, 2024
Accepted: July 24, 2024
Published: August 6, 2024





component system, a number of factors can influence the magnitude of interfacial adsorption. The results from a series of surface-tension-based analyses of AWI adsorption demonstrate that the AWI adsorption of PFAS is enhanced by the longer chain and higher solution ionic strength. ^{21–23} As surfactants, the dissolved PFAS in soil water can reduce surface tension and decrease capillary forces, ^{21,24,25} which can affect partially saturated water flow and soil water distribution when their concentrations are above a certain threshold. In turn, the retardation of the PFAS transport is decreased. Additionally, the adsorption at soil—water interfaces can be strongly correlated to the organic carbon fraction ^{26–30} and the process can be either rate-limited or nonlinear. ²⁰

Mathematical models of PFAS transport in the vadose zone have been developed, and a more quantitative analysis of the physical and chemical processes of PFAS transport has been conducted. Shin et al.^{31,32} simulated perfluorooctanoate (PFOA) transport in the vadose zone using the U.S. EPA Pesticide Root Zone Model, version 3(PRZM-3), but AWI adsorption was not included in the model. Later on, a onedimensional (1D) mathematical model incorporating ratelimited solid-phase adsorption and AWI adsorption was developed and applied to simulate the break-through curves of perfluorooctanesulfonic acid (PFOS) and PFOA in soil-/ sand-packed column experiments under unsaturated conditions.³³ These mathematical models focus on the PFAS transport under the steady-state partially saturated flow condition. Thus, no effect of the transient flow is included. Considering the AWI area and distribution are significantly impacted under the transient flow state and the following effects on PFAS transport, the mathematical models for the PFAS transport under transient partially saturated flow in the vadose zone have been developed.^{20,34} Additionally, these models explicitly account for the change in surface tension by dissolved PFAS as well as PFAS adsorption at both air-water interfaces and solid-phase surfaces. The results of these models demonstrate that AWI adsorption of PFAS is a significant source of retention (e.g., 1-2% PFAS in pore water after infiltrating the vadose zone), and fine-texture materials could have a lower retardation factor than coarse materials because of higher retained water content, which indicates fewer AWIs for adsorbing PFAS. 20,34,35 This form of adsorption is not always the dominant retention process. Compared to AWI adsorption, the contribution of solid-phase adsorption can be considerable in many sites when the vadose zone is contaminated.^{20,36} Later on, the model was also used to investigate the heterogeneity effects in two-dimensional (2D) and three-dimensional (3D) conditions, with results displaying preferential flow caused by subsurface heterogeneity-accelerated leaching of PFAS, especially for long-chain PFAS, and this phenomenon is more prominent than conventional contaminants due to the destruction of AWIs. 35,37

While previous studies above have focused on the vadose zone as a critical source of PFAS contamination, surface water is also a main source contributing to PFAS contamination in the groundwater. Surface water and groundwater interact within the hyporheic zone along river corridors. Therefore, PFAS in surface water can reach groundwater by mixing processes within the riverbed and bank. To date, no modeling studies on PFAS transport under a transient surface water—groundwater interaction scenario have been reported. Even though the studies on PFAS transport in the vadose zone demonstrate that AWI adsorption and solid-phase surface

adsorption play significant roles in PFAS retention, whether they have the same influences when PFAS transport occurs during the surface water—groundwater interactions is still unclear. In addition, our knowledge of the impact of sediment heterogeneity on PFAS transport is also limited.

The sensitivity of PFAS transport to the various physical and chemical processes in the subsurface and the properties of sediments are critical aspects to consider. The parameters related to these processes and sediment properties can affect PFAS retention. As a result, it is desirable to identify which parameters are the most critical to controlling PFAS transport. The insights into the importance of these parameters will help improve the quantitative evaluation of PFAS risks and provide practical and effective guidance for managing and mitigating PFAS contamination risk in the environment.

This study focuses on the global sensitivity analysis (GSA) to explore the effects of sediments' physical and chemical properties on PFAS transport in heterogeneous riparian sediments influenced by surface water-groundwater interactions. In order to investigate the heterogeneity effects, five heterogeneous layouts combining low- and high-permeability sediments (i.e., facies types as per Soltanian and Ritzi⁴⁰) in varied proportions are generated, and the proportion values based on the natural riparian sediment characteristics were presented by Wallace et al. 41 We combined an in-house PFAS transport solver based on PFLOTRAN (i.e., state-of-the-art massively parallel subsurface flow and reactive transport code)⁴² with the statistical methods in PSUADE⁴³ to simulate 2000 scenarios for each proportion of high-permeability sediment. By examining a broad range of chosen property parameters, such as the porosity of each sediment, residual saturation, and adsorption coefficient of the solid phase, we will gain a detailed comprehension of which parameters are the most critical for PFAS transport in natural heterogeneous geological media. Our findings will be critical for evaluating the environmental and public health risks caused by PFAS transport from surface water to groundwater as a drinking water source, thereby decreasing the long-term drinking water safety risks and preserving groundwater resources. Ultimately, this study has the potential to not only identify critical factors of PFAS transport in the riverbed and bank but also provide valuable insights that can guide the development of remediation strategies and inform future research on PFAS transport along the river corridor and watershed.

■ METHODOLOGY

Conceptual Model. The heterogeneous riparian sediment layouts were generated using the method in Wallace et al., 44,45 in which they investigate the controlling factors of how sediment heterogeneity influences nitrogen dynamics near tidal rivers. The lithologic data for generating the heterogeneous were originally collected from the Christina River Basin Critical Zone Observatory, suited in the fifth-oder tidal freshwater zone of White Clay Creek, Delaware, in the study of Musial et al.46 The drilling samples collected from the floodplain and riverbed show that the consolidated sediments consist of low-permeable (LP) facies (i.e., mud) and highpermeable facies (i.e., sand and gravel). In the architectures in the study of Wallace et al., 44,45 a series of 2D sedimentary architectures consisting of LP and high-permeable (HP) sediments were generated using a Markov Chain approach and indicator simulation with quenching in T-PROGS,4 geostatistical software. T-PROGS creates stochastic simula-

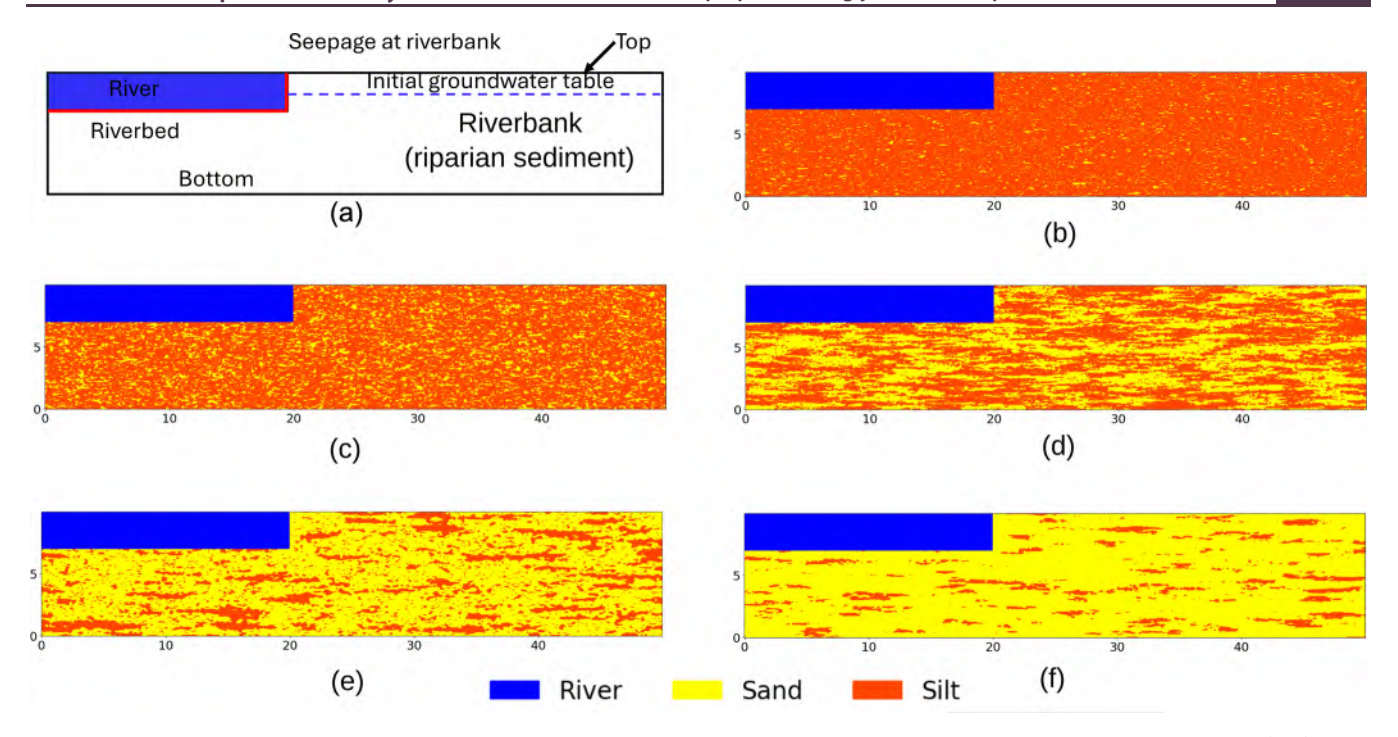


Figure 1. Two-dimensional simulation domain design and heterogeneous layouts with different proportions between high-permeable (HP) facies and low-permeable (LP) facies. (a) Simulation domain settings, (b) riparian sediments with 10% HP facies, (c) riparian sediments with 25% HP facies, (d) riparian sediments with 50% HP facies, (e) riparian sediments with 75% HP facies, and (f) riparian sediments with 90% HP facies.

tions of geological structures utilizing a transition probability approach to characterize the spatial distribution of geological variables based on their transitional probabilities. The T-PROGS output is a set of N material sets on a 3D grid. This method incorporates the physical sediment characteristics, including mean lengths and volume proportions. Each facies has distinct properties, such as permeability, porosity, solidphase adsorption coefficient, and residual saturation. To integrate the surface water-groundwater interactions, as shown in Figure 1a, the upper left area of the simulation domain is a river, and a sine function is implemented to change the water stage periodically. To include the heterogeneity effects on PFAS transport and retention processes, five layouts, whose volume proportion of high-permeability sediment is 10, 25, 50, 75, and 90%, respectively, are used (Figure 1b-f). This allows us to understand the effect of preferential flow pathways on PFAS fate and transport. It is known that volume proportion controls the facies's connectivity, 48-52 and here, the HP facies having 75 and 90% volume proportion are fully connected. The dimension of the entire simulation domain is 50 m \times 10 m, and the river area is 20 m \times 10 m. PFOS in surface water reaches groundwater through the seepage and transport in riparian sediment. Considering water table fluctuations caused by river stage changes, transport of a PFAS is described by physical processes of advection and dispersion as well as chemical processes of solid-phase sorption and adsorption to air-water interfaces under the partially saturated flow condition. In our model, the flow field is solved by the Richards equation first. Then, the updated saturation and flow velocity fields are used to solve the PFAS transport processes. Previous studies have shown that solid-phase adsorption is a primary process of potential importance for PFAS transport in porous media, especially for cationic and zwitterionic PFAS species, because of the electrostatic attraction to negatively charged organic matter or clays. 20,53

In addition, the adsorption at air—water interfaces has been shown to be the other primary source of the retention of PFAS during transport in partially saturated porous media for infiltration scenarios. Therefore, these two adsorption processes are implemented to include their potential effects on PFAS transport.

A relatively high initial concentration in the river was selected to better explore the impacts of physical and chemical heterogeneity on the PFOS fate and transport. This represents a conservative case to study the maximum possible PFOS sorption in the solid phase and at air—water interfaces (AWIs). This approach facilitates a clearer understanding of PFOS dynamics under high contamination levels, though the model's applicability extends to lower concentrations, with sorption values expected to remain consistent until the point where available sorption sites are not fully occupied by PFOS molecules.

Mathematical Models. Partially Saturated Flow and Transport of PFAS. As riparian sediments are usually partially saturated, the flow through partially saturated porous formation is computed by solving the Richards equation in PFLOTRAN^{41,54,55}

$$\frac{\partial}{\partial t}(nS_{\rm w}\eta) + \nabla \bullet (\eta \mathbf{q}) = 0 \tag{1}$$

with the Darcy flux defined as

$$\mathbf{q} = \frac{-kk_{\rm r}}{\mu}\nabla(P - \rho_{\rm w}\mathbf{g}z) \tag{2}$$

where n is the porosity of the porous medium, $S_{\rm w}$ is the water saturation, η is the molar water density (kmol·m⁻³), ${\bf q}$ is the Darcy flux (m·s⁻¹), P is the pressure (kg·m⁻¹·s⁻²), ${\bf g}$ is the gravity (m·s⁻²), ${\bf z}$ is the spatial coordinate in the direction of the gravitational force (m), ${\bf k}$ is the intrinsic permeability (m²),

and $k_{\rm r}$ is the relative permeability and approximated by an empirical function from the Van Genuchten equations 56

$$k_{\rm r} = S_{\rm w,e}^{0.5} [1 - (1 - S_{\rm w,e}^{1/m})^m]^2$$
(3)

where m is the fitting parameter and $S_{\rm w,e} = \frac{\theta - \theta_{\rm r}}{\theta_{\rm s} - \theta_{\rm r}}$ is the effective water saturation ($\theta_{\rm s}$ is the saturated water content; $\theta_{\rm r}$ is the residual water content).

To calculate the volumetric water content, we use the function from the Van Genuchten equation as^{56}

$$\theta = \begin{cases} \theta_{\rm r} + \frac{\theta_{\rm s} - \theta_{\rm r}}{\left[1 + (\alpha |h|)^n\right]^m}, & m = 1 - \frac{1}{n}, \quad h < 0\\ \theta_{\rm s}, & h \ge 0 \end{cases}$$
(4)

where α (1/m) and n are fitting parameters and $\theta_{\rm r}$ and $\theta_{\rm s}$ are the residual and saturated water contents, respectively.

The transport and retention of PFAS in the sediments are described by an advection—dispersion equation coupled with adsorption at the solid surface and AWI in 34,35

$$\frac{\partial(\theta C)}{\partial t} + \rho_{b} \frac{\partial C_{s}}{\partial t} + \frac{\partial C_{aw}}{\partial t} + \nabla \bullet (\theta \mathbf{v} C) - \nabla \bullet (\theta \mathbf{D} \nabla C)$$

$$= 0 \tag{5}$$

where C is the aqueous concentration of PFAS (mol·m⁻³), ρ_b is the bulk density of the sediment (kg·m⁻³), and \mathbf{v} is the vector of the interstitial pore water velocity (m·s⁻¹) ($\mathbf{v} = \mathbf{q}/\theta$), where \mathbf{q} is the Darcy flux that is computed from eq 2. C_s is the solid-phase adsorption (mol· kg), C_{aw} is the AWI adsorption (mol·m⁻³), and \mathbf{D} is the hydrodynamic dispersion tensor (m²·s⁻¹), and the sum of the mechanical dispersion and molecular diffusion coefficients (m²·s⁻¹) is given by

$$\mathbf{D} = \alpha_{\mathrm{T}} |\mathbf{v}| \mathbf{I} + (\alpha_{\mathrm{L}} - \alpha_{\mathrm{T}}) \frac{\mathbf{v} \mathbf{v}^{\mathrm{T}}}{|\mathbf{v}|} + \tau D_{0} \mathbf{I}$$
(6)

where I is the identity matrix, $\alpha_{\rm L}$ and $\alpha_{\rm T}$ are longitude and transverse dispersivities (m), respectively, D_0 is the molecular diffusion coefficient in water (m²·s⁻¹), and $\tau = \frac{\theta^{7/3}}{\theta_{\rm s}^2}$ is the tortuosity factor in sediment. Based on the prior experiment results, the solid-phase adsorption is modeled by nonlinear, Freundlich isotherm adsorption

$$C_{\rm s} = K_{\rm f} C^N \tag{7}$$

where K_f and N are fitting parameters to experimental data. The AWI adsorption C_{aw} is described as

$$C_{\rm aw} = A_{\rm aw} \Gamma = A_{\rm aw} K_{\rm aw} C \tag{8}$$

where K_{aw} is the AWI adsorption coefficient (m) and A_{aw} is the AWI area (m⁻¹), and it is parametrized as the water saturation

$$A_{\rm aw} = x_2 S_{\rm w}^2 + x_1 S_{\rm w} + x_0 (9)$$

where x_2 , x_1 , and x_0 are fitting parameters from the measurements of interfacial tracer experiments. The AWI adsorption coefficient $K_{\rm aw}$ is determined using the Gibbs adsorption equation with the ideal dilute solution assumption 57,58

$$K_{\rm aw} = \frac{\Gamma}{C} = \frac{1}{RTC} \left(\frac{\partial \sigma}{\partial \ln C} \right)_T \tag{10}$$

Surface tension σ is a function of the aqueous concentration C, which is calculated by the Szyszkowski equation ^{59,60}

$$\sigma = \sigma_0 \left[1 - b \ln \left(1 + \frac{C}{a} \right) \right] \tag{11}$$

where $a \pmod{1}$ and b are fitting parameters from experimental data. Substituting eq 11 into eq 10 obtains³⁴

$$K_{\text{aw}} = \frac{1}{RT} \frac{\sigma_0 b}{a + C} \tag{12}$$

where R is the universal gas constant (J·K⁻¹·mol⁻¹), T is the temperature (K). After substitution of eqs 7 and 8 to eq 5, the equation for the PFAS transport in partially saturated porous media with the solid-phase and AWI adsorption processes

$$\frac{\partial(\theta C)}{\partial t} + \rho_{b} \frac{\partial(K_{f}C^{N})}{\partial t} + \frac{\partial(A_{aw}K_{aw}C)}{\partial t} + \frac{\partial}{\partial x}(\theta \nu C)
- \frac{\partial}{\partial x} \left(\theta D \frac{\partial C}{\partial x}\right)$$

$$= 0$$
(13)

To simulate the PFAS transport and retention in riparian sediment, eq 1 for partially saturated flow and eq 13 are fully coupled in PFLOTRAN. For eq 13, a sandbox solver of PFLOTRAN was developed in-house. Both equations are discretized using the finite volume approach in PFLOTRAN.

Monte Carlo (MC) Simulations. To analyze the effects of hydrological and geochemical parameters on the flow and PFAS transport, we used PSUADE, an uncertainty quantification tool, to generate and sample the chosen independent variables for Monte Carlo simulations. Each chosen variable was generated by the distribution with the designated range shown in the table. However, a specific statistical distribution is not enough to guarantee that the desired information can be obtained with the number of samples. Therefore, PSUADE provides sampling methods to help users maximize the amount of desired information that can be extracted from the output data. We need to do the responsive surface analysis (RSA), which explores the relationships between designated explanatory variables to one or more outcome variables using Latin hypercube sampling (LHS). The LHS method divides the range of each parameter into equally probable intervals and then randomly samples the values in each interval, ensuring even coverage of the parameter space. 43,61,62 A sample of size mr is generated as the equation below 43,63

$$\mathbf{m}_i = [x_{i1}, x_{i2}, ..., x_{i,mX}], \quad i = 1, 2, ..., mr$$
 (14)

where \mathbf{x} is the uncertain parameters, mX is the number of parameters in \mathbf{x} , and mr is the sample size. Each variable range is exhaustively divided into disjoint intervals of equal probability, and each value is selected randomly from each interval. 61

Uncertainty and Sensitivity Analyses. While the Monte Carlo (MC) simulation provides us with a comprehensive understanding of each parameter's range and variability, it does not directly illustrate the degree to which each parameter influences the results. Consequently, to ascertain the impact of each input parameter on the simulation results and identify the most prominent ones, conducting uncertainty and sensitivity analyses is critical. PSUADE offers robust functions for implementing variance-based sensitivity analysis methods. These methods are able to identify significant parameters in

the modeling process and quantify their relative contributions, enabling us to determine which parameters have a substantial impact on the simulation results.

To quantify the uncertainty and global sensitivity of input parameters, we employ the multivariate adaptive regression spline (MARS) method, which is a flexible, nonparametric approach that constructs piece-wise linear regression models over the domain of predictor variables, facilitating a nuanced understanding of parameter behavior. The variance of conditional expectation (VCE) is utilized in conjunction with MARS to assess the global sensitivity. The VCE is given by 65,66

$$VCE(X_i) = \frac{100}{k} \sum_{j=1}^{k} (\overline{Y}_j - \overline{Y})^2 - \frac{1}{ks^2} \sum_{j=1}^{k} \sum_{i=1}^{s} (Y_{ij} - Y_j)^2$$
(15)

where VCE represents the variability in the conditional expected values of the output variable Y, X_i symbolizes the uncertain input parameters, k denotes the number of distinct values for each input parameter, and s signifies the number of replications. The input parameters' importance is evaluated using eq 15 and then reranked based on the MARS importance ranking (from 0 to 100).

Additionally, we apply RSA, a statistical and mathematical technique that simplifies models influenced by multiple independent variables. RSA elucidates the relationships between combinations of predictor variables and an outcome variable in a 2D or 3D space, providing valuable predictions of the response. This method is particularly useful in scenarios in which the outcome variable is influenced by a multitude of interacting factors, allowing us to visualize and understand the complex relationships and dependencies among these variables.

The combination of VCE, MARS, and RSA provides indepth uncertainty and sensitivity analyses, leading to a more robust understanding of the primary factors influencing PFAS transport and retention in heterogeneous riparian sediments.

Initial and Boundary Conditions of Numerical Simulations. The initial water table is set at 7.6 m. The area above the water table is unsaturated with the minimum residual water content of HP and LP facies ($\theta_{r,\text{HP}}$ and $\theta_{r,\text{LP}}$). The boundary conditions for the domain boundaries are the hydrostatic pressure boundary conditions. The hydrostatic pressure at each cell of the boundary is defined as

$$p_i(z_i, t) = p_0(t) - \rho_i g(z_i - z_0)$$
(16)

where p_i is the pressure at cell i, p_0 is the atmosphere pressure at the water table, ρ_i is the fluid density at cell i, z_0 is the water level, and z_i is the coordinate value of cell i along the aquifer thickness. For the riverbank and riverbed, the value of p_0 fluctuates with a sine function shown in Figure 1a. However, it is kept as constant 101,325 Pa for others. The top and border of the domain are set to be the no-flow and free-flow boundary conditions, respectively.

For the transport part, the constant concentration at each cell of the boundary

$$C_i(\mathbf{x}, t) = C_0 \tag{17}$$

where C_i is the PFOS concentration at each cell of the boundary, \mathbf{x} is the coordinate of each cell on the boundary, and C_0 is the assigned constant PFOS concentration for the boundary. The initial PFOS concentration in riparian sediments is 0 mol/L.

Parameters and Data. In this study, we employ perfluorooctanesulfonic acid (PFOS) as the PFAS contaminant in surface water, as it is a dominant PFAS compound. In total, we choose eight parameters of LP and HP facies to investigate which can substantially affect PFOS transport and retention in heterogeneous riparian sediments. The ranges of their values and variations, as shown in Table 1, are from field and

Table 1. Uncertain Parameters and Objective Functions for PFAS Transport in a Riparian Sediment

| | minimum | maximum | mean | distribution type |
|--|---------|---------|--------|----------------------|
| Hydraulic and Transport Parameters | | | | |
| HP facies porosity (n_h) | 0.25 | 0.53 | 0.38 | lognormal |
| LP facies porosity (n_l) | 0.4 | 0.7 | 0.541 | lognormal |
| surface tension | 0.0528 | 0.071 | 0.0622 | normal |
| in HP facies $(\sigma_h, N/m)$ | | | | |
| surface tension | 0.0528 | 0.071 | 0.0624 | normal |
| in LP facies $(\sigma_{l'}, N/m)$ | | | | |
| $ \begin{array}{c} HP \; facies \; adsorption \\ (K_{f,h}) \end{array} $ | 0.055 | 0.381 | 0.223 | normal |
| coefficient | | | | |
| LP facies adsorption $(K_{f,l})$ | 0.055 | 0.381 | 0.221 | normal |
| coefficient | | | | |
| residual saturation in HP facies $(\theta_{ m h,r})$ | 0.01 | 0.069 | 0.0385 | normal |
| residual saturation in LP facies $(\theta_{ m l,r})$ | 0.118 | 0.294 | 0.228 | normal |
| Objective Functions | | | | |
| PEOS amount in the aqueous phase (mol) | | | | |

PFOS amount in the aqueous phase (mol)

PFOS amount at air-water interfaces (AWIs) (mol)

PFOS amount at the solid-phase surface (mol)

ratio of PFOS amount in HP facies

laboratory work in refs 33,36,67, and 68. Using these parameters and other parameters from McGarr et al.⁶⁹ in PFLOTRAN, we coupled PFLOTRAN and PSUADE to run a set of MC simulations of PFOS transport in heterogeneous riparian sediments having different proportions of high-permeable sediment (Figure 1). The permeability of each sediment is calculated using the Kozeny–Carman equation^{70,71}

$$k = C \frac{n^3}{\rho_s^2 S_s^2 (1+n)} \tag{18}$$

where C is a constant for taking into account the tortuosity in porous media, ρ_s is the density of the solid phase (kg·m⁻³), S_s is the specific surface (m²·kg⁻¹) of the solid phase, and n is porosity. To evaluate the effects of the chosen physical and chemical parameters of each sediment on PFOS transport and retention, four objective functions listed in Table 1 are defined to postprocess the results of MC simulations. LHS in PSUADE is used to sample each chosen parameter from its distribution for 2000 PFLOTRAN simulations. The postprocessed results from the objective functions are used as the input for PSUADE to conduct GSA with MARS and RSA with bootstrap aggregating (bagging) as described.

For the values of α and m in the Van Genuchten equations (eq 3 and 4), we used $\alpha = 0.00124$ for HP facies and $\alpha = 0.001$ for LP facies.³⁴ The values of N in eq 7 for the solid-phase adsorption are 0.85 and 0.81 for HP and LP facies, respectively.³⁴

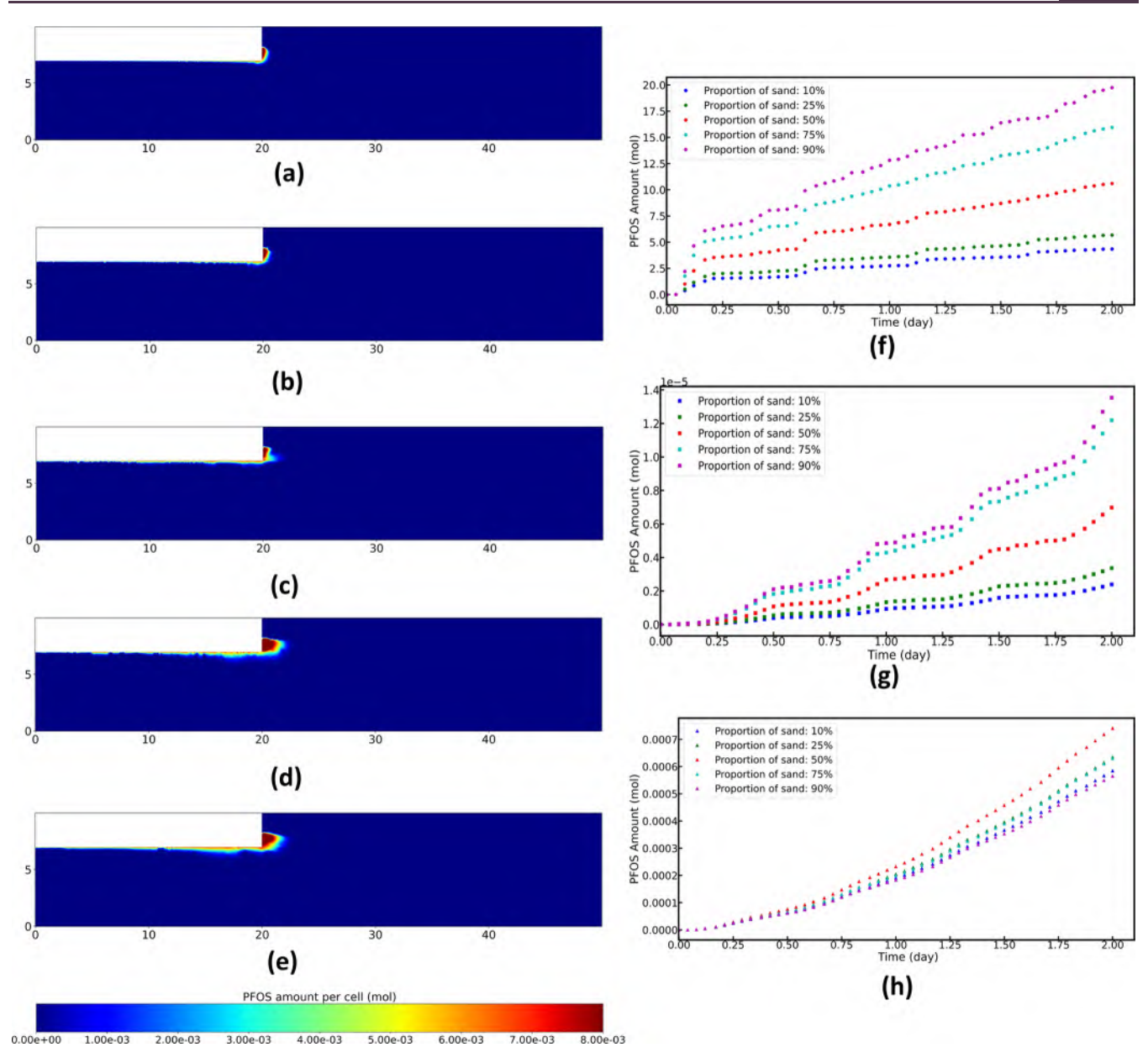


Figure 2. PFOS distribution in five heterogeneous layouts after 2 days and the median values of PFOS amount in three phases during the simulations with different volume proportions of HP facies: (a) volume proportion of HP facies is 10%, (b) volume proportion of HP facies is 25%, (c) volume proportion of HP facies is 50%, (d) volume proportion of HP facies is 75%, (e) volume proportion of HP facies is 90%, (f) median of PFOS amount in the aqueous phase for five heterogeneous layouts, (g) median of PFOS amount at AWI for five heterogeneous layouts, and (h) median of PFOS amount at the solid-phase surface for five heterogeneous layouts.

RESULTS

The numerical solver for PFAS transport in the subsurface was verified compared to the data from the laboratory experiments (the verification results are in the Supporting Information. The simulation results are compared to the data in the study of Brusseau et al. ⁷²). The results show that PFOS was transported further when the volume proportion of HP facies increased (Figure 2a,b). After analyzing the amount of PFOS in different phases, it is observed that most PFOS from the river is not kept either at the AWI or solid-phase surface but in groundwater. As shown in Figure 2f—h, compared to the range of the PFOS amount in groundwater, which is 10^0-10^1 mol, the PFOS amounts at the AWI and solid-phase surface are significantly low $(10^{-5}-10^{-6}$ mol for the PFOS at AWI; 10^{-4} mol for the PFOS at the solid-phase surface). This is different from the

results of the simulations for PFAS infiltration in the vadose zone in refs 34,35, and 73, which demonstrate that the vast majority of PFOS in the vadose zone is retained at AWIs with only 1–2% PFOS being found in the aqueous phase. For simulations presented here, more than 99% of PFOS is in groundwater, and the percentage of PFAS adsorbed at AWI is almost negligible in all five heterogeneous layouts, as shown in Figure 1. This difference is attributed to the reduced AWI area created in riparian sediments during the surface watergroundwater interactions. Moreover, when the volume proportion of HP sediment (e.g., sand) increases, the amount of PFOS in the aqueous phase and adsorbed at AWIs increases as well. However, the amount of PFOS adsorbed at the solid-phase surface follows a different trend (Figure 2h), with the most observed in the 50% sand fraction and the least 10 and

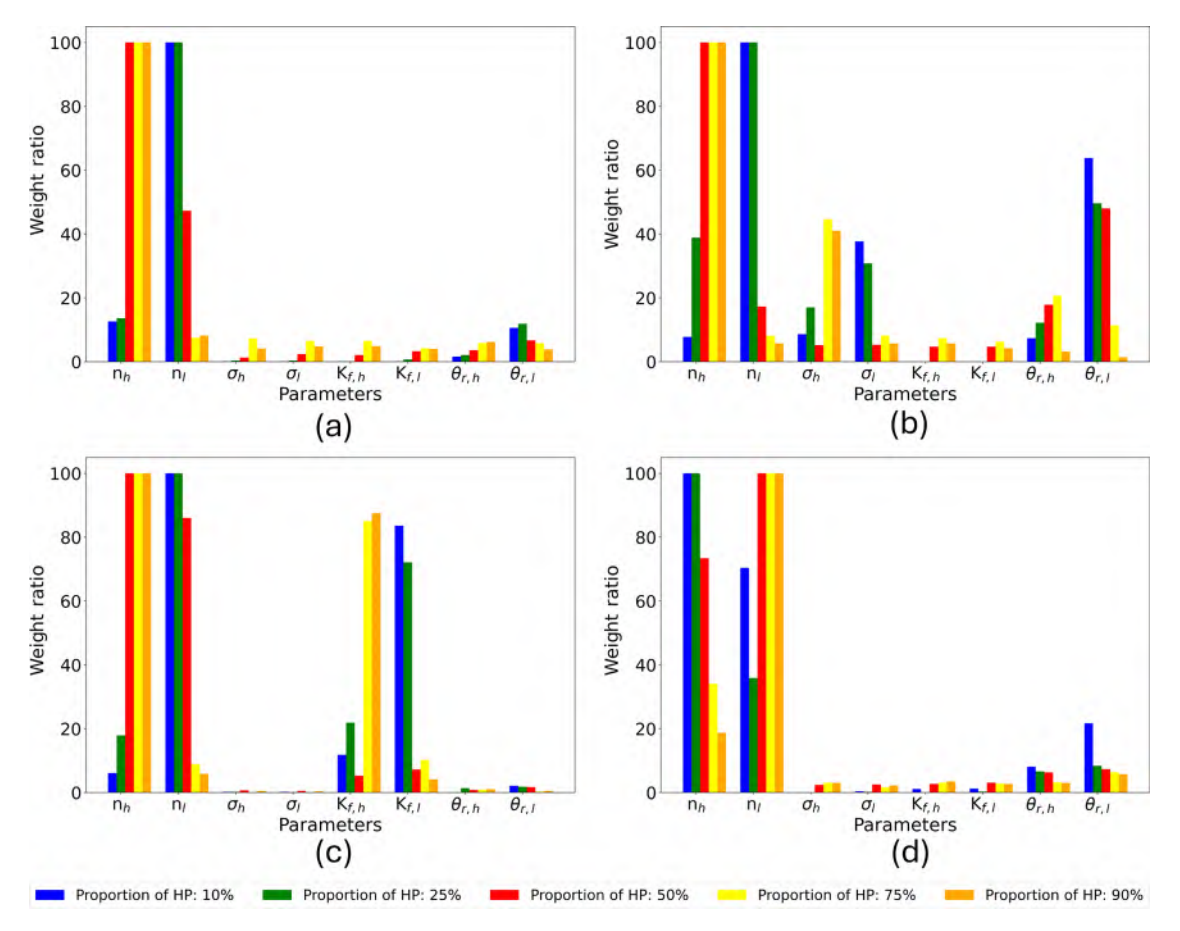


Figure 3. Global sensitivity analysis of the objective functions to eight uncertain parameters in Table 1 using the MARS method. (a) PFOS amount in the aqueous phase (groundwater), (b) PFOS amount at AWIs, (c) PFOS amount at the solid-phase surface, and (d) normalized PFOS amount in HP facies.

90% HP sediment (sand). This indicates that the maximum PFOS adsorption at the solid phase requires connectivity to both the PFOS source and adsorption sites.

Global Sensitivity Analysis. The findings above demonstrate that the sediment architecture and heterogeneity dictate PFOS transport and fate in riparian sediments. There is still a need to understand the systematic influence of the hydraulic and geochemical properties of each sediment. Here, we mainly focus on the influence of chosen parameters over the amount of PFOS in the aqueous phase, PFOS adsorbed at the solid-phase surface, and its distribution in each facies. These further investigation results include not only the GSA on the importance of each hydraulic and geochemical parameter but also 1D/2D RSA on how the most dominant parameters interact with each other to determine PFOS transport and fate in riparian sediments. The GSA results provide the detailed influence score rank of the chosen parameters.

The results of this analysis are visually presented in Figure 3a-d, which illustrates the sensitivity of the amount of PFOS in the aqueous phase, PFOS adsorbed at the air—water interface (AWI) and solid-phase surface, and normalized PFOS amount in HP and LP sediments, respectively. The most striking insight that can be gleaned from the figure is the significant sensitivity of PFOS transport over the porosities of HP and LP sediments, whose scores of MARS are often 100 or nearly 100, and their permeabilities correlated to the porosities, especially for the PFOS in the aqueous phase (Figure 3a). In Figure 3b, the results display that the porosities of LP and HP

facies are still the dominant factor in the adsorption of PFOS at AWI, but the second most dominant factor shifts from surface tension in HP facies to the residual saturation value of LP facies with the volume proportion of HP facies decreasing. Figure 3c shows that the solid-phase adsorption coefficient of HP sediment plays the second most important role in the adsorption of PFOS at the solid-phase surface when the volume proportion of HP sediment is high and low (90, 75, 25, and 10%). Only when the volume proportion is the median value (50%) do the porosities of two sediments have the strongest influence. For the PFOS distribution in each facies, the porosity of LP sediment is always the most dominant factor without the dependence on the HP sediment volume proportion (Figure 3d).

Response Surface Analysis. To understand the potential correlations between the parameters listed in Table 1 and the PFOS amount and distribution in riparian sediments, a robust approach utilizing two-dimensional (2D) RSA is employed. This technique is complemented by the use of MARS coupled with the bootstrapping aggregating method. This approach is applied to analyze the postprocessing results of each 2000 simulations for each heterogeneous layouts in Figure 1.

The experimental data of MC simulations and prediction data from RSA for each heterogeneous sediment layout are fitted by linear regression. Figure 4 shows the results on PFOS amount in the aqueous phase, at AWIs and solid-phase surface, and the PFOS ratio in HP facies when the volume proportion of HP facies is 90%. R^2 values for the actual MC simulation and

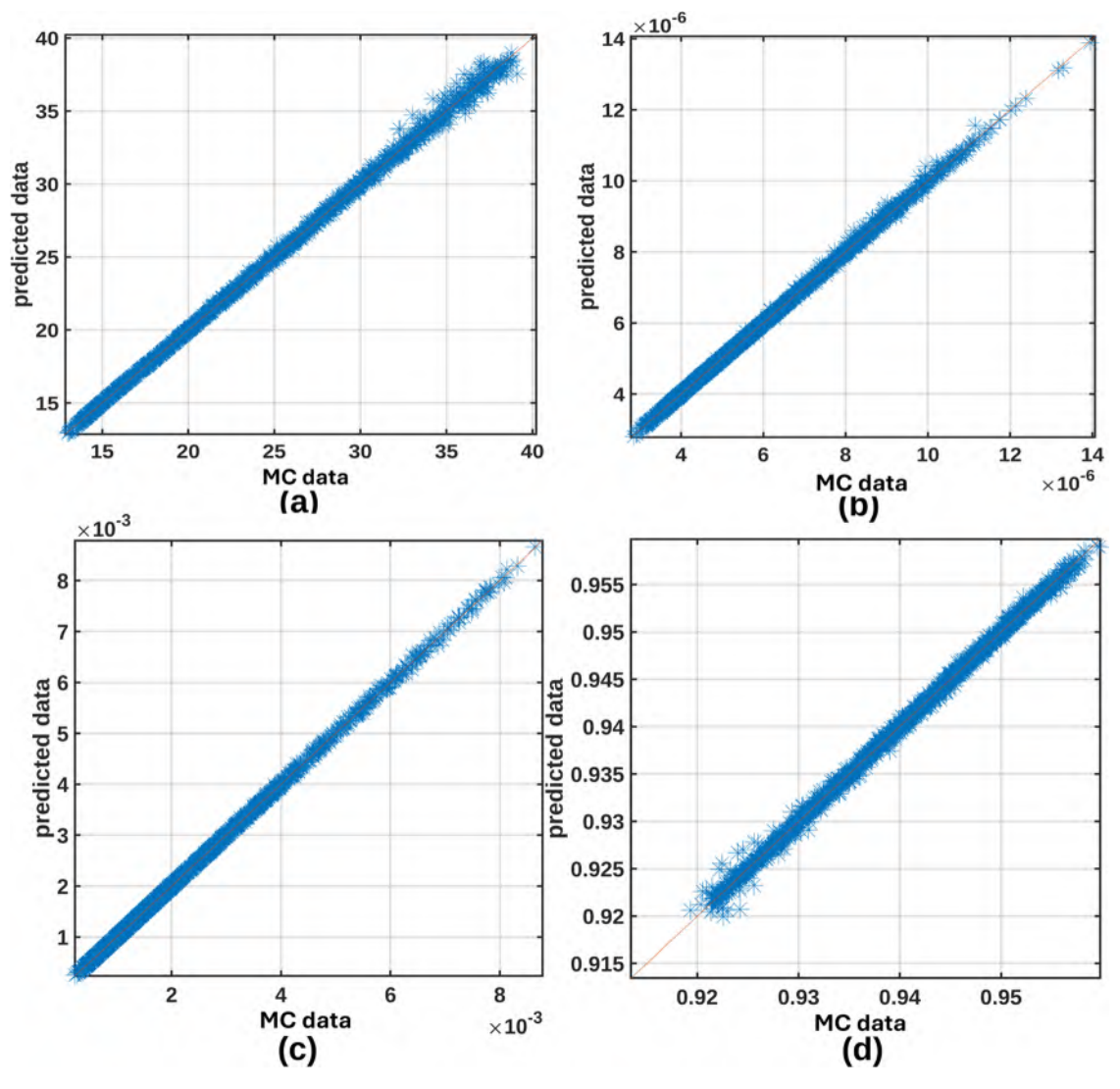


Figure 4. Relevant results of regression generating response surfaces for (a) PFOS amount in the aqueous phase, (b) PFOS amount at AWIs, (c) PFOS amount at the solid-phase surface, and (d) PFOS ratio in HP facies, when the volume proportion of HP facies is 90%.

the predicted response surface model data are 0.9996, 0.9983, 0.9983, and 0.9983, respectively. Thus, the response surface models can accurately predict the PFOS amount in the aqueous phase, at AWIs and solid-phase surface, and the ratio of PFOS amount in HP facies. For the left heterogeneous layout, all of the fits of objective functions in Table 1 keep almost the same accuracy as those for the layout in which the volume proportion of HP facies is 90%. Their figures and R^2 values are given in the Supporting Information.

Based on the GSA results in Figure 3, we chose the most influential parameters for each objective function in Table 1 to run 2D RSA. The objective is to elucidate the correlations between chosen parameters and each objective function, as shown in Figures 5 and 6.

Figures 5a,e,i and 6a present the correlations between the PFOS amount in the aqueous phase and two parameters: n_h and n_l . Clearly, the porosities of both sediments dictate the maximum amount of PFOS in the aqueous phase. When both of them reached their maximum values, which indicates that the permeabilities of the two facies both reached their maxima, the amount of PFOS in the aqueous phase reached the highest level as well (about 1.8-42 mol, depending on the

heterogeneous layout). This trend is caused by the fact that more surface water with PFOS can enter the groundwater when both facies have higher porosities/permeabilities. In the five heterogeneous layouts, the porosities of the two facies affected the PFOS amount most significantly, except in the layout in which the volume proportion of HP facies is 10%, where the second prominent parameter is the residual saturation in LP (Figure 6f).

For the PFOS amount at air—water interfaces, when the volume proportion of HP facies is higher than 0.5, the maximum of PFOS adsorbed at AWIs reaches around 6.5×10^{-5} and 4.2×10^{-5} mol individually with the maximum values of θ_h and n_h (Figure Sb,f). When the volume proportion of HP facies is 0.5, the second prominent parameter becomes the residual saturation in LP (θ_l) (Figure Sj). With its minimum (0.118) and the maximum of n_h (0.53), the amount of PFOS adsorbed at AWIs reaches its maximum (1.40 \times 10⁻⁵ mol). When the volume proportion of HP facies decreases to 25 and 10%, n_l replaces the role of n_h (Figure 6b,f). The minimum of θ_l (0.118) and the maximum of n_l (0.7) cause the maximum of PFOS at AWI (about 4.6×10^{-6} and 3.6×10^{-6} mol).

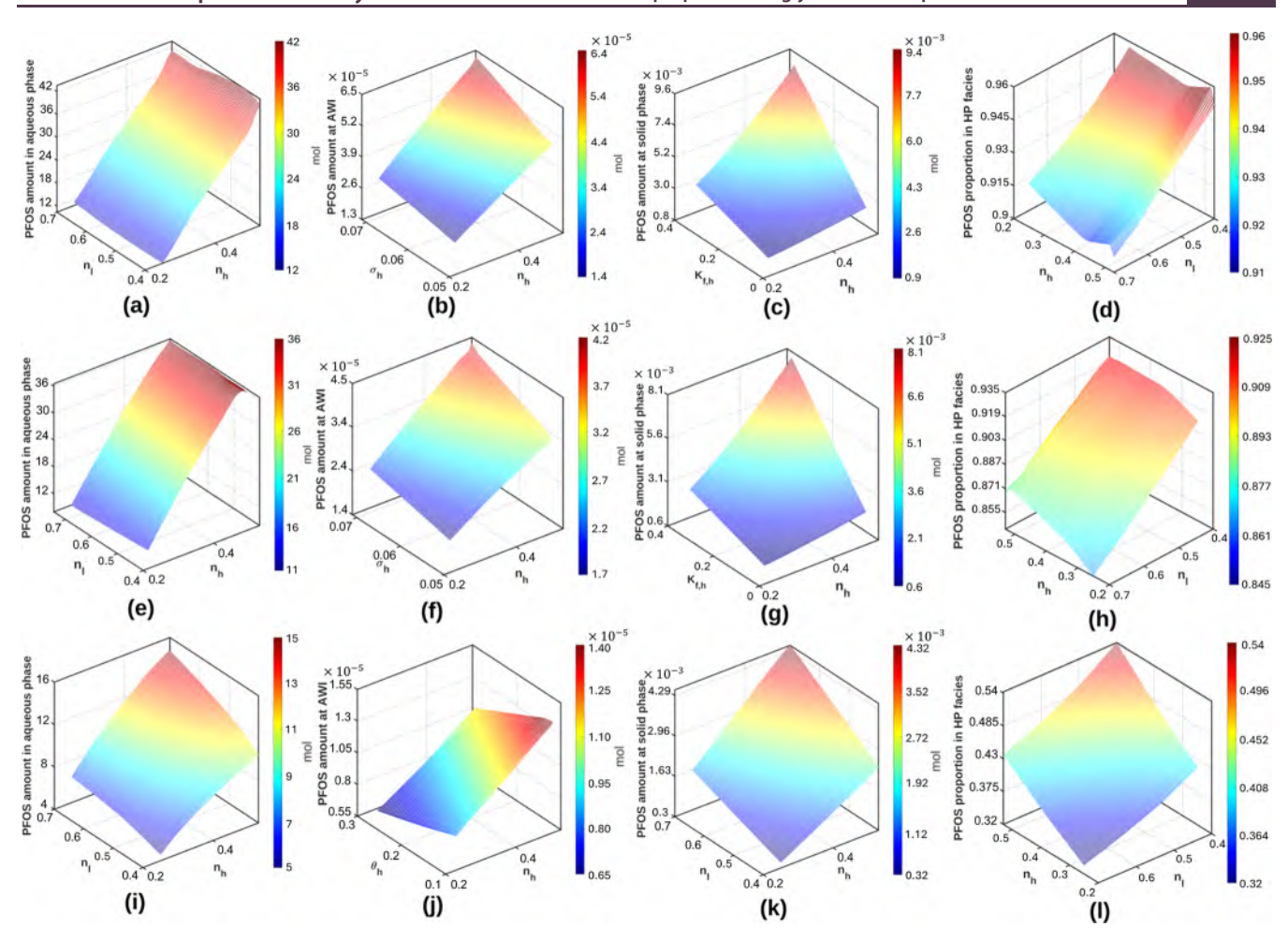


Figure 5. Two-dimensional RSA plots for the amount of PFOS in the aqueous phase, at AWIs, and solid-phase surface and the ratio of PFOS amount in HP facies, respectively, with the volume proportion of HP facies being 90, 75, and 50%.

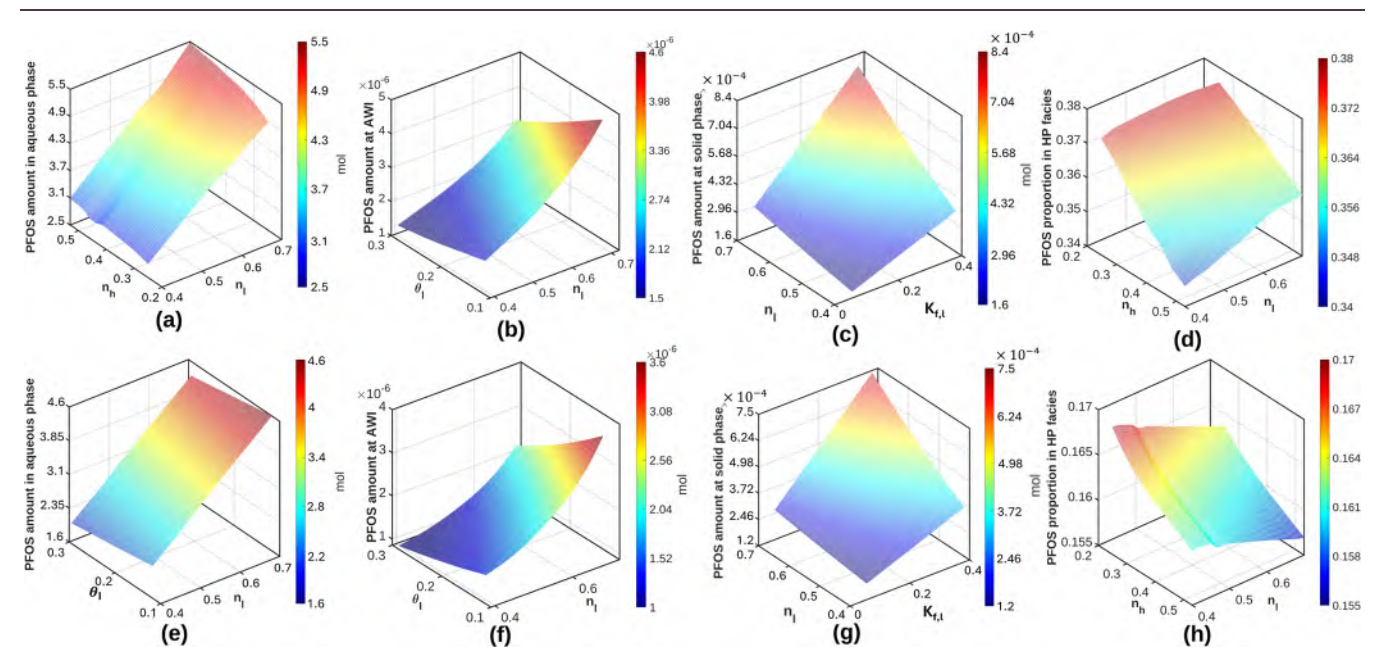


Figure 6. (Continued from Figure 5) Amount of PFOS in the aqueous phase, at AWIs, and solid-phase surface and the ratio of PFOS amount in HP facies, respectively, with the volume proportion of HP facies being 25 and 10%.

For the PFOS amount at the solid-phase surface, the porosity of HP (n_h) and the adsorption coefficient of the HP

surface (K_h^t) have a monotonic correlation with the amount of adsorbed PFOS before the volume proportion of HP facies

decreasing to 0.5 (Figure 5c,g). When both parameters are at their maximum values (n_h = 0.53 and $K_{\rm f,l}$ = 0.384), the amount of PFOS adsorbed at the solid-phase surface reaches its maximum (about 9.4 × 10⁻³ and 8.1 × 10⁻³ mol). In contrast, the minimum amount of PFOS adsorbed is about 9.0 × 10⁻⁴ and 6.1 × 10⁻⁴ mol, respectively, when n_h and $K_{\rm d}^l$ reach their minima (0.25 and 0.055). Although Figure 5k shows a trend similar to that of Figure 5c,g, the second influential parameter is replaced by the porosity of the LP surface. After the volumetric proportion of HP facies becomes 25 and 10%, both influential parameters shift to be the porosity of LP and the adsorption coefficient of the LP surface (Figure 6c,g). The amount of PFOS adsorbed at the solid-phase surface decreases to the range between 1.2 × 10⁻⁵ to 8.4 × 10⁻⁴ mol.

Shifting our focus to the PFOS amount ratio in HP facies (Figure 5d,h,k), the higher the porosity of the HP facies but the lower the porosity of the LP facies, the more PFOS is in the HP facies. In contrast, when the volumetric proportion of LP facies is dominant (Figure 6d,h), the lowest HP porosity (0.25) leads to the highest PFOS ratio in HP facies (0.345 and 0.135). Notably, to maximize the PFOS ratio in the HP facies of all of the layouts (0.96, 0.925, 0.54, 0.38, and 0.17 individually), the porosity of LP facies needs to be the minimum in its range (0.4) in most conditions. Similarly, for the minimum of the PFOS ratio in the HP facies, the porosity of LP facies goes in the opposition direction and reaches its maximum (0.7).

DISCUSSION

Compared to recent laboratory and modeling studies on PFOS fate and transport in the vadose zone, the simulation results presented here (Figure 2) appear to be contradictory. This is because the accumulated PFOS amount at AWIs is orders of magnitude less than that of what is in the aqueous phase and adsorbed at the solid particle surface (10⁻⁵ vs 10⁰-10¹ and 10⁻⁴ mol). However, simulations in prior studies were conducted under completely different scenarios. For instance, laboratory experiments and modeling work in refs 33-35,72, and 74 investigated surficial discharge and vertical leaching of PFAS through the vadose zone to groundwater. The results show that adsorption at air-water and solid-water interfaces leads to strong retention of PFAS in the vadose zone. In these studies, the entire domain where PFAS transport and retention occur is partially saturated. The simulations presented here examined a river as a PFOS source of riparian sediments, including the riverbed and bank, through surface watergroundwater interactions. As the river stage fluctuates, as Figure S1 presents, the groundwater table near the river fluctuates as well. The groundwater table fluctuation causes the saturation of the affected area to fluctuate. These repeated saturation changes create partially saturated flow conditions and air-water interfaces (AWIs) to absorb PFAS. With the fluctuation continuing, more PFOS is transported from the river to the groundwater and then absorbed at the AWIs (Figure 2g). Additionally, when there are more HP facies, the area affected by the river stage fluctuation and having partially saturated flow is larger; therefore, there is more PFAS adsorbed at the AWIs. Hence, the PFOS AWIs accumulation increase is accompanied by increasing HP facies's proportion (Figure 2g). However, the area that is affected by the river stage fluctuation and where partially saturated flow occurs is quite limited. As a result, most PFOS is transported in the aqueous phase (water; Figure 2f). If there is a surface discharge

source on the floodplain, it is likely that more PFOS would have accumulated at AWIs in partially saturated sediments. This could be a good future study extending this work.

The riparian sediment heterogeneity determines the mass of PFOS transported from river to groundwater. The PFOS amount in the aqueous phase and at AWIs is dictated by the volume proportion of HP facies (Figure 2f,g). When the volume proportion increases, HP facies are more connected, creating preferential flow pathways and a higher exchange amount. Therefore, more PFOS is transported from the river to groundwater. In addition, PFOS travels further through the floodplain, and the impacted area increases. Therefore, more PFOS is adsorbed at AWIs. In contrast, the results of PFOS adsorption at the solid-phase surface (Figure 2h) demonstrated that adsorption requires a combination of both spatial connectivity of HP facies and sites favorable to PFOS adsorption on LP facies surfaces. When HP facies are fully connected with a high proportion of LP facies along those preferential flow paths, the amount of PFOS adsorption at the solid-phase surface can reach its peak. Clearly, sedimentary architecture plays an important role in PFOS transport and its affected area in the floodplain. Previous works on the fate and transport of nonreactive solutes and organic contaminants (e.g., sorptive solutes such as perchloroethylene (PCE)) have shown that subsurface transport in sedimentary aquifers cannot be well understood without characterizing and parsimoniously representing physical and chemical heterogeneities across ⁷ This is also the case for prior studies focusing on the nutrient dynamics in riparian floodplains. For instance, Wallace et al.⁷⁸ simulated subsurface N₂O production from a heterogeneous riparian floodplain. Their results highlight that accurate lithologic representation is imperative for characterizing subsurface biogeochemistry along the river corridor.

By applying our sensitivity analysis framework, we obtain more insights into which parameters are critical for the PFOS transport process. As shown in Figure 3, the porosities of two facies, which determine their permeabilities by eq 18, are often the most influential parameters to the amount of PFOS in different phases and at interfaces, especially in the aqueous phase. These parameters represent intrinsic physical properties of sedimentary facies types and largely remain constant over time, which indicates that the means of decreasing the PFOS amount and affected area significantly in riparian sediments can only be either decreasing the PFOS concentration in surface water as the source or lowering the porositypermeability of sediments. Conversely, the sensitivity and uncertainty analyses on vertical leaching of PFAS through the vadose zone conducted by Zeng et al. 73 demonstrated that the strength of retention increases with the increase of the PFOS chain, higher ionic strengths, and lower applied concentration, and the results of PFAS transport are the most sensitive to the parameters related to the adsorption at different interfaces. These parameters (e.g., Freundlich exponent N and the airwater interfacial area) are dynamic parameters affected by environmental conditions, such as temperature, surfactant concentration, and surface minerals. Therefore, the fluctuation degree of these parameters is substantially based on local environmental changes, potentially exerting an impact on PFOS retention and mobility in the vadose zone. The point is that although the studies of Zeng et al.73 and ours look at PFAS/PFOS, the nature of boundary conditions, which is essentially surface infiltration via the river, shows significant differences in terms of what needs to be characterized or

prioritized in terms of characteristics and input parameters to reduce model uncertainty. In the cases presented in Brusseau et al., ⁷⁴ Brusseau, ³³ Guo et al., ³⁴ Brusseau et al., ⁷² Zeng and Guo, ³⁵ and Zeng et al., ⁷³ attention to well characterize AWI parameters as the most important parameters has been highlighted. Our study can be viewed as an extension of the studies on PFOS transport and retention in different hydrological scenarios.

Note that our simulations consider the Richards equation to solve groundwater flow and do not capture PFAS trapped in the pore space if PFAS exists as a separate phase (i.e., a surfactant). In such conditions, three-phase flow needs to be solved with water, air, and PFAS/surfactant represented as each phase, respectively. As a result, constitutive relations with respect to each phase, such as capillarities and relative permeabilities, need to be incorporated so that PFAS entrapment can be fully captured. Though this is outside the scope of this study, and the authors are not aware of any data sets to parametrize such models, our computational model can be extended to include the mathematical formulations of this three-phase flow process.

CONCLUSIONS

We present an integrated framework that focuses on the PFOS transport and retention processes in heterogeneous riparian sediments during the surface water—groundwater interactions and controlling parameters. In this framework, the validated numerical model is employed to investigate the primary parameters controlling the PFOS transport and retention behavior using Monte Carlo simulation and sensitivity and uncertainty analyses. For PFOS transport under the specific scenario, surface water—groundwater interactions, our conclusions are summarized below:

- 1. This study demonstrates that, in general, the porosity of sedimentary facies, which is correlated to the permeability, is the most crucial parameter for PFOS transport in heterogeneous riparian sediments during surface water—groundwater interactions. Although the GSA shows that the other parameters of riparian sediment have certain degrees of influence on PFOS transport and retention, the response surface analyses show that the effects of the physical properties of HP facies and LP facies (ie., porosities) are dominant, and the effect of other parameters mainly depends on the volume proportion of HP facies, which indicates the spatial connectivity of the preferential path for PFOS transport.
- 2. The results on the PFOS distribution in HP and LP facies and analysis of the influential parameters imply that the role of the LP facies in storing PFOS cannot be neglected, especially when the volume proportions of LP and HP facies are almost the same. This phenomenon results in the transport of PFOS and the PFOS released from LP facies, leading to long-term PFOS retention.

Further exploration of this framework could also be adapted to include more types of PFAS, geochemical parameters (e.g., pH, ionic strength, surface charge of the solid phase), as well as other types of physical parameters (e.g., thermal conductivity) in riparian sediments. For instance, the framework can be adapted to include the rate-limited interfacial partitioning and non-Fickian transport effects in partially saturated flow conditions. Additionally, it would also be worthwhile to validate and refine the framework with multiple PFAS/PFOS

transports, heterogeneity from other geographic regions, and climate conditions, such as investigating anionic, zwitterionic, and cationic PFASs' transport, to investigate their retention processes under the conditions having different amounts of charged organic matter or clay in riparian sediment. It is possible that the dominant factor may vary depending on the specific PFAS (e.g., anionic, zwitterionic, and cationic PFAS), hydrological scenario (e.g., surface water-groundwater interactions, infiltration from vadose zone), spatial heterogeneity from other geographical regions, and climate conditions. The importance of this work is the rank of these chosen parameters through global sensitivity analysis and responsive analysis. So, based on our results and sampling ranges of values, we can be confident that the physical heterogeneity is the dominant factor for PFAS transport in riparian sediment than other parameters of chemical properties (e.g., solid-phase adsorption coefficient) under the surface water-groundwater interaction conditions.

ASSOCIATED CONTENT

Supporting Information

The Supporting Information is available free of charge at https://pubs.acs.org/doi/10.1021/acsearthspace-chem.4c00037.

Additional figures of the river stage fluctuation implemented in our simulations and validation cases for our PFAS transport solver (PDF)

AUTHOR INFORMATION

Corresponding Authors

Pei Li — Department of Geosciences, University of Cincinnati, Cincinnati, Ohio 45221, United States; orcid.org/0009-0005-8885-1911; Email: lip6@ucmail.uc.edu

Mohamad Reza Soltanian — Department of Geosciences and Department of Environmental Engineering, University of Cincinnati, Cincinnati, Ohio 45221, United States; Email: soltanma@ucmail.uc.edu

Authors

Jeffery T. McGarr — Department of Geosciences, University of Cincinnati, Cincinnati, Ohio 45221, United States

Farzad Moeini — Department of Geosciences, University of Cincinnati, Cincinnati, Ohio 45221, United States

Zhenxue Dai — College of Construction Engineering, Jilin University, Changchun, Jilin 130026, China; orcid.org/0000-0002-0805-7621

Complete contact information is available at: https://pubs.acs.org/10.1021/acsearthspacechem.4c00037

Notes

The authors declare no competing financial interest.

ACKNOWLEDGMENTS

This research was supported by the National Science Foundation under grants EAR-2048452. Any opinions, findings, conclusions, or recommendations expressed in this article are those of the authors and do not necessarily reflect those of the National Science Foundation. All of the simulation input files and related data files are shared at http://www.hydroshare.org/resource/851a3458b717469a948a26fad24c6b53.

REFERENCES

- (1) Ahrens, L. Polyfluoroalkyl compounds in the aquatic environment: a review of their occurrence and fate. *J. Environ. Monit.* **2011**, 13, 20–31.
- (2) Hatton, J.; Holton, C.; DiGuiseppi, B. Occurrence and behavior of per- and polyfluoroalkyl substances from aqueous film-forming foam in groundwater systems. *Biorem. J.* **2018**, *28*, 89–99.
- (3) Prevedouros, K.; Cousins, I. T.; Buck, R. C.; Korzeniowski, S. H. Sources, fate and transport of perfluorocarboxylates. *Environ. Sci. Technol.* **2006**, *40*, 32–44.
- (4) Wallis, I.; Hutson, J.; Davis, G.; Kookana, R.; Rayner, J.; Prommer, H. Model-based identification of vadose zone controls on PFAS mobility under semi-arid climate conditions. *Water Res.* **2022**, 225, No. 119096.
- (5) McGarr, J. T.; Mbonimpa, E. G.; McAvoy, D. C.; Soltanian, M. R. Fate and Transport of Per-and Polyfluoroalkyl Substances (PFAS) at Aqueous Film Forming Foam (AFFF) Discharge Sites: A Review. *Soil Syst.* **2023**, *7*, No. 53.
- (6) OECD. Toward a New Comprehensive Global Database of Perand Polyfluoroalkyl Substances (PFASs); OECD, 2018.
- (7) Cordner, A.; Goldenman, G.; Birnbaum, L. S.; Brown, P.; Miller, M. F.; Mueller, R.; Patton, S.; Salvatore, D. H.; Trasande, L. The True Cost of PFAS and the Benefits of Acting Now. *Environ. Sci. Technol.* **2021**, *55*, 9630–9633.
- (8) Brusseau, M. L.; Anderson, R. H.; Guo, B. PFAS concentrations in soils: Background levels versus contaminated sites. *Sci. Total Environ.* **2020**, 740, No. 140017.
- (9) Xu, B.; Liu, S.; Zhou, J. L.; Zheng, C.; Weifeng, J.; Chen, B.; Zhang, T.; Qiu, W. PFAS and their substitutes in groundwater: Occurrence, transformation and remediation. *J. Hazard. Mater.* **2021**, 412, No. 125159.
- (10) Johnson, G. R.; Brusseau, M. L.; Carroll, K. C.; Tick, G. R.; Duncan, C. M. Global distributions, source-type dependencies, and concentration ranges of per- and polyfluoroalkyl substances in groundwater. *Sci. Total Environ.* **2022**, *841*, No. 156602.
- (11) Gefell, M. J.; Huang, H.; Opdyke, D.; Gustafson, K.; Vlassopoulos, D.; McCray, J. E.; Best, S.; Carey, M. Modeling PFAS Fate and Transport in Groundwater, with and Without Precursor Transformation. *Groundwater* **2022**, *60*, 6–14.
- (12) Mahinroosta, R.; Senevirathna, L. The effectiveness of PFAS management options on groundwater quality in contaminated land using numerical modelling. *Chemosphere* **2021**, *279*, No. 130528.
- (13) Abunada, Z.; Alazaiza, M. Y.; Bashir, M. J. An Overview of Perand Polyfluoroalkyl Substances (PFAS) in the Environment: Source, Fate, Risk and Regulations. *Water* **2020**, *12*, No. 3590.
- (14) Krafft, M. P.; Riess, J. G. Per- and polyfluorinated substances (PFASs): Environmental challenges. *Curr. Opin. Colloid Interface Sci.* **2015**, 20, 192–212.
- (15) Rayne, S.; Forest, K. Perfluoroalkyl sulfonic and carboxylic acids: A critical review of physicochemical properties, levels and patterns in waters and wastewaters, and treatment methods. *J. Environ. Sci. Health, Part A: Toxic/Hazard. Subst. Environ. Eng.* **2009**, 44, 1145–1199.
- (16) Dauchy, X.; Boiteux, V.; Colin, A.; Hémard, J.; Bach, C.; Rosin, C.; Munoz, J.-F. Deep seepage of per-and polyfluoroalkyl substances through the soil of a firefighter training site and subsequent groundwater contamination. *Chemosphere* **2019**, 214, 729–737.
- (17) Høisæter, Å.; Pfaff, A.; Breedveld, G. D. Leaching and transport of PFAS from aqueous film-forming foam (AFFF) in the unsaturated soil at a firefighting training facility under cold climatic conditions. *J. Contam. Hydrol.* **2019**, 222, 112–122.
- (18) Hunter Anderson, R.; Adamson, D. T.; Stroo, H. F. Partitioning of poly-and perfluoroalkyl substances from soil to groundwater within aqueous film-forming foam source zones. *J. Contam. Hydrol.* **2019**, 220, 59–65.
- (19) Brusseau, M. L.; Yan, N.; Glubt, S. V.; Wang, Y.; Chen, W.; Lyu, Y.; Dungan, B.; Carroll, K. C.; Holguin, F. O. Comprehensive retention model for PFAS transport in subsurface systems. *Water Res.* **2019**, *148*, 41–50.

- (20) Silva, J. A. K.; Šimunek, J.; McCray, J. E. A Modified HYDRUS Model for Simulating PFAS Transport in the Vadose Zone. *Water* **2020**, *12*, No. 2758.
- (21) Lyu, Y.; Brusseau, M. L.; Chen, W.; Yan, N.; Fu, X.; Lin, X. Adsorption of PFOA at the Air-Water Interface during Transport in Unsaturated Porous Media. *Environ. Sci. Technol.* **2018**, *52*, 7745–7753
- (22) Schaefer, C. E.; Drennan, D. M.; Tran, D. N.; Garcia, R.; Christie, E.; Higgins, C. P.; Field, J. A. Measurement of Aqueous Diffusivities for Perfluoroalkyl Acids. *J. Environ. Eng.* **2019**, *145*, No. 06019006.
- (23) Silva, J.; McCray, J.; Martin, W. Final Report: Baseline Data Acquisition and Numerical Modeling to Evaluate the Fate and Transport of PFAS within the Vadose Zone, SERDP Project ER18-1389; Strategic Environmental Research and Development Program (SERDP), 2020. Available online: https://www.serdp-estcp.org/Program-Areas/Environmental-Restoration/Contaminated-Groundwater/Emerging-Issues/ER18%E2%88%921389 (accessed Sept 10, 2020).
- (24) Brusseau, M. L.; Glubt, S. V. The influence of surfactant and solution composition on PFAS adsorption at fluid-fluid interfaces. *Water Res.* **2019**, *161*, 17–26.
- (25) Silva, J. A.; Martin, W. A.; Johnson, J. L.; McCray, J. E. Evaluating air-water and NAPL-water interfacial adsorption and retention of Perfluorocarboxylic acids within the Vadose zone. *J. Contam. Hydrol.* **2019**, 223, No. 103472.
- (26) Guelfo, J. L.; Higgins, C. P. Subsurface transport potential of perfluoroalkyl acids at aqueous film-forming foam (AFFF)-impacted sites. *Environ. Sci. Technol.* **2013**, *47*, 4164–4171.
- (27) Milinovic, J.; Lacorte, S.; Vidal, M.; Rigol, A. Sorption behaviour of perfluoroalkyl substances in soils. *Sci. Total Environ.* **2015**, *511*, 63–71.
- (28) Du, Z.; Deng, S.; Bei, Y.; Huang, Q.; Wang, B.; Huang, J.; Yu, G. Adsorption behavior and mechanism of perfluorinated compounds on various adsorbents review. *J. Hazard. Mater.* **2014**, 274, 443–454.
- (29) Campos Pereira, H.; Ullberg, M.; Kleja, D. B.; Gustafsson, J. P.; Ahrens, L. Sorption of perfluoroalkyl substances (PFASs) to an organic soil horizon Effect of cation composition and pH. Chemosphere 2018, 207, 183–191.
- (30) Xiao, F.; Jin, B.; Golovko, S. A.; Golovko, M. Y.; Xing, B. Sorption and Desorption Mechanisms of Cationic and Zwitterionic Per- And Polyfluoroalkyl Substances in Natural Soils: Thermodynamics and Hysteresis. *Environ. Sci. Technol.* **2019**, *53*, 11818–11827.
- (31) Shin, H. M.; Vieira, V. M.; Ryan, P. B.; Detwiler, R.; Sanders, B.; Steenland, K.; Bartell, S. M. Environmental fate and transport modeling for perfluorooctanoic acid emitted from the Washington works facility in West Virginia. *Environ. Sci. Technol.* **2011**, *45*, 1435–1442
- (32) Shin, H. M.; Ryan, P. B.; Vieira, V. M.; Bartell, S. M. Modeling the air-soil transport pathway of perfluorooctanoic acid in the mid-Ohio Valley using linked air dispersion and vadose zone models. *Atmos. Environ.* **2012**, *51*, 67–74.
- (33) Brusseau, M. L. Simulating PFAS transport influenced by rate-limited multi-process retention. *Water Res.* **2020**, *168*, No. 115179.
- (34) Guo, B.; Zeng, J.; Brusseau, M. L. A Mathematical Model for the Release, Transport, and Retention of Per- and Polyfluoroalkyl Substances (PFAS) in the Vadose Zone. *Water Resour. Res.* **2020**, *56*, No. e2019WR026667.
- (35) Zeng, J.; Guo, B. Multidimensional simulation of PFAS transport and leaching in the vadose zone: Impact of surfactant-induced flow and subsurface heterogeneities. *Adv. Water Resour.* **2021**, *155*, No. 104015.
- (36) Brusseau, M. L. Estimating the relative magnitudes of adsorption to solid-water and air/oil-water interfaces for per- and poly-fluoroalkyl substances. *Environ. Pollut.* **2019**, 254, No. 113102.
- (37) Zeng, J.; Guo, B. Reduced Accessible Air-Water Interfacial Area Accelerates PFAS Leaching in Heterogeneous Vadose Zones. *Geophys. Res. Lett.* **2023**, *50*, No. e2022GL102655.

- (38) Xiao, F.; Simcik, M. F.; Halbach, T. R.; Gulliver, J. S. Perfluorooctane sulfonate (PFOS) and perfluorooctanoate (PFOA) in soils and groundwater of a U.S. metropolitan area: Migration and implications for human exposure. *Water Res.* 2015, 72, 64–74.
- (39) Liu, Z.; Lu, Y.; Wang, T.; Wang, P.; Li, Q.; Johnson, A. C.; Sarvajayakesavalu, S.; Sweetman, A. J. Risk assessment and source identification of perfluoroalkyl acids in surface and ground water: Spatial distribution around a mega-fluorochemical industrial park, China. *Environ. Int.* **2016**, *91*, 69–77.
- (40) Soltanian, M. R.; Ritzi, R. W. A new method for analysis of variance of the hydraulic and reactive attributes of aquifers as linked to hierarchical and multiscaled sedimentary architecture. *Water Resour. Res.* **2014**, *50*, 9766–9776.
- (41) Wallace, C. D.; Tonina, D.; McGarr, J. T.; de Barros, F. P. J.; Soltanian, M. R. Spatiotemporal dynamics of nitrous oxide emission hotspots in heterogeneous riparian sediments. *Water Resour. Res.* **2021**, *57*, No. e2021WR030496, DOI: 10.1029/2021WR030496.
- (42) Hammond, G. E.; Lichtner, P. C.; Mills, R. T. Evaluating the performance of parallel subsurface simulators: An illustrative example with PFLOTRAN. *Water Resour. Res.* **2014**, *50*, 208–228.
- (43) Douglas-Smith, D.; Iwanaga, T.; Croke, B. F.; Jakeman, A. J. Certain trends in uncertainty and sensitivity analysis: An overview of software tools and techniques. *Environ. Modell. Software* **2020**, *124*, No. 104588.
- (44) Wallace, C. D.; Sawyer, A. H.; Barnes, R. T.; Soltanian, M. R.; Gabor, R. S.; Wilkins, M. J.; Moore, M. T. A model analysis of the tidal engine that drives nitrogen cycling in coastal riparian aquifers. *Water Resour. Res.* **2020**, *56*, No. e2019WR025662.
- (45) Wallace, C. D.; Sawyer, A. H.; Soltanian, M. R.; Barnes, R. T. Nitrate removal within heterogeneous riparian aquifers under tidal influence. *Geophys. Res. Lett.* **2020**, *47*, No. e2019GL085699.
- (46) Musial, C. T.; Sawyer, A. H.; Barnes, R. T.; Bray, S.; Knights, D. Surface water-groundwater exchange dynamics in a tidal freshwater zone. *Hydrol. Processes* **2016**, *30*, 739–750.
- (47) Carle, S. F.T-PROGS: Transition ProbabilityGeostatistical Software Version 2.1; Lawrence Livermore National Laboratory, 2007.
- (48) Stauffer, D.; Aharony, A. Introduction to Percolation Theory; CRC Press, 1994.
- (49) Gershenzon, N. I.; Soltanian, M.; Ritzi, R. W.; Dominic, D. F. Understanding the impact of open-framework conglomerates on water-oil displacements: the Victor interval of the Ivishak Reservoir, Prudhoe Bay Field, Alaska. *Pet. Geosci.* **2015**, *21*, 43–54, DOI: 10.1144/petgeo2014-017.
- (50) Soltanian, M. R.; Amooie, M. A.; Dai, Z.; Cole, D.; Moortgat, J. Critical dynamics of gravito-convective mixing in geological carbon sequestration. *Sci. Rep.* **2016**, *6*, No. 35921.
- (51) Liu, Y.; Wallace, C. D.; Zhou, Y.; Ershadnia, R.; Behzadi, F.; Dwivedi, D.; Xue, L.; Soltanian, M. R. Influence of streambed heterogeneity on hyporheic flow and sorptive solute transport. *Water* **2020**, *12*, No. 1547.
- (52) Ershadnia, R.; Hajirezaie, S.; Amooie, A.; Wallace, C. D.; Gershenzon, N. I.; Hosseini, S. A.; Sturmer, D. M.; Ritzi, R. W.; Soltanian, M. R. CO2 geological sequestration in multiscale heterogeneous aquifers: Effects of heterogeneity, connectivity, impurity, and hysteresis. *Adv. Water Resour.* **2021**, *151*, No. 103895.
- (53) Nickerson, A.; Rodowa, A. E.; Adamson, D. T.; Field, J. A.; Kulkarni, P. R.; Kornuc, J. J.; Higgins, C. P. Spatial trends of anionic, zwitterionic, and cationic PFASs at an AFFF-impacted site. *Environ. Sci. Technol.* **2021**, *55*, 313–323.
- (54) Hammond, G.; Lichtner, P.et al. PFLOTRAN: Reactive Flow & Transport Code for Use on Laptops to Leadership-Class Supercomputers. *Groundwater Reactive Transport Models*; Bentham Science Books, 2012.
- (55) Wu, R.; Chen, X.; Hammond, G.; Bisht, G.; Song, X.; Huang, M.; Niu, G.-Y.; Ferre, T. Coupling surface flow with high-performance subsurface reactive flow and transport code PFLOTRAN. *Environ. Modell. Software* **2021**, *137*, No. 104959.

- (56) Van Genuchten, M. T. A closed-form equation for predicting the hydraulic conductivity of unsaturated soils. *Soil Sci. Soc. Am. J.* **1980**. *44*. 892–898.
- (57) Kim, H.; Rao, P. S. C.; Annable, M. D. Determination of effective air-water interfacial area in partially saturated porous media using surfactant adsorption. *Water Resour. Res.* **1997**, 33, 2705–2711.
- (58) Brusseau, M. L. Assessing the potential contributions of additional retention processes to PFAS retardation in the subsurface. *Sci. Total Environ.* **2018**, *613–614*, 176–185.
- (59) Chang, C.-H.; Franses, E. I. Adsorption dynamics of surfactants at the air/water interface: a critical review of mathematical models, data, and mechanisms. *Colloids Surf., A* **1995**, *100*, 1–45.
- (60) Adamson, A. W.; Gast, A. P.et al. *Physical Chemistry of Surfaces*; Interscience Publishers: New York, 1967; Vol. 150.
- (61) Dai, Z.; Stauffer, P. H.; Carey, J. W.; Middleton, R. S.; Lu, Z.; Jacobs, J. F.; Hnottavange-Telleen, K.; Spangler, L. H. Pre-site characterization risk analysis for commercial-scale carbon sequestration. *Environ. Sci. Technol.* **2014**, *48*, 3908–3915.
- (62) Ren, W.; Dai, H.; Yuan, S.; Dai, Z.; Ye, M.; Soltanian, M. R. Global sensitivity study of non-reactive and sorptive solute dispersivity in multiscale heterogeneous sediments. *J. Hydrol.* **2023**, 619, No. 129274.
- (63) Jia, S.; Dai, Z.; Yang, Z.; Du, Z.; Zhang, X.; Ershadnia, R.; Soltanian, M. R. Uncertainty quantification of radionuclide migration in fractured granite. *J. Cleaner Prod.* **2022**, *366*, No. 132944.
- (64) Dauchy, X.; Boiteux, V.; Colin, A.; Hémard, J.; Bach, C.; Rosin, C.; Munoz, J. F. Deep seepage of per- and polyfluoroalkyl substances through the soil of a firefighter training site and subsequent groundwater contamination. *Chemosphere* **2019**, 214, 729–737.
- (65) Ren, W.; Ershadnia, R.; Wallace, C. D.; LaBolle, E. M.; Dai, Z.; de Barros, F. P.; Soltanian, M. R. Evaluating the effects of multiscale heterogeneous sediments on solute mixing and effective dispersion. *Water Resour. Res.* **2022**, 58, No. e2021WR031886.
- (66) Du, Z.; Dai, Z.; Yang, Z.; Jia, S. Uncertainty and sensitivity analysis of radionuclide migration through fractured granite aquifer. *J. Environ. Radioact.* **2022**, 255, No. 107020.
- (67) Brusseau, M. L. The influence of molecular structure on the adsorption of PFAS to fluid-fluid interfaces: Using QSPR to predict interfacial adsorption coefficients. *Water Res.* **2019**, *152*, 148–158.
- (68) Brusseau, M. L. Influence of chain length on field-measured distributions of PFAS in soil and soil porewater. *J. Hazard. Mater. Lett.* **2023**, *4*, No. 100080.
- (69) McGarr, J. T.; Li, P.; Meyal, A.; Moeini, F.; Rubenstein, R.; Versteeg, R.; Wallace, C. D.; Soltanian, M. R. Fate and transport of per- and polyfluoroalkyl substances within heterogenous riparian floodplains *Sci. Total Environ.*, 2024.
- (70) Chapuis, R. P.; Aubertin, M. On the use of the Kozeny Carman equation to predict the hydraulic conductivity of soils. *Can. Geotech. J.* **2003**, *40*, 616–628.
- (71) Wang, M.; Wang, J.; Xu, G.; Zheng, Y.; Kang, X. Improved model for predicting the hydraulic conductivity of soils based on the Kozeny-Carman equation. *Hydrol. Res.* **2021**, *52*, 719–733.
- (72) Brusseau, M. L.; Guo, B.; Huang, D.; Yan, N.; Lyu, Y. Ideal versus Nonideal Transport of PFAS in Unsaturated Porous Media. *Water Res.* **2021**, 202, No. 117405.
- (73) Zeng, J.; Brusseau, M. L.; Guo, B. Model validation and analyses of parameter sensitivity and uncertainty for modeling long-term retention and leaching of PFAS in the vadose zone. *J. Hydrol.* **2021**, *603*, No. 127172.
- (74) Brusseau, M. L.; Khan, N.; Wang, Y.; Yan, N.; Glubt, S. V.; Carroll, K. C. Nonideal Transport and Extended Elution Tailing of PFOS in Soil. *Environ. Sci. Technol.* **2019**, *53*, 10654–10664.
- (75) Soltanian, M. R.; Ritzi, R. W.; Huang, C. C.; Dai, Z. Relating reactive solute transport to hierarchical and multiscale sedimentary architecture in a L agrangian-based transport model: 1. Time-dependent effective retardation factor. *Water Resour. Res.* **2015**, *51*, 1586–1600.
- (76) Soltanian, M. R.; Ritzi, R. W.; Huang, C. C.; Dai, Z. Relating reactive solute transport to hierarchical and multiscale sedimentary

architecture in a L agrangian-based transport model: 2. Particle displacement variance. Water Resour. Res. 2015, 51, 1601–1618.

- (77) Soltanian, M. R.; Behzadi, F.; de Barros, F. P. Dilution enhancement in hierarchical and multiscale heterogeneous sediments. *J. Hydrol.* **2020**, *587*, No. 125025.
- (78) Wallace, C. D.; Tonina, D.; McGarr, J. T.; de Barros, F. P.; Soltanian, M. R. Spatiotemporal dynamics of nitrous oxide emission hotspots in heterogeneous riparian sediments. *Water Resour. Res.* **2021**, *57*, No. e2021WR030496.